**Solid Earth
Discussions**

Application of titanium-in-quartz thermobarometry to greenschist facies veins and recrystallized quartzites in the Hsüehshan range, Taiwan

S. Kidder[1,*], J.-P. Avouac[1], and Y.-C. Chan[2]

[1]California Institute of Technology, Pasadena, CA, USA
[2]Academia Sinica, Taipei, Taiwan
[*]now at: University of Otago, New Zealand

Correspondence to: S. Kidder (steven.kidder@otago.ac.nz)

Discussion Paper | Discussion Paper | Discussion Paper | Discussion Paper

SED
4, 663–706, 2012

Application of titanium-in-quartz thermobarometry

S. Kidder et al.

Title Page

Abstract | Introduction
Conclusions | References
Tables | Figures

◄ | ►►
◄ | ►

Back | Close

Full Screen / Esc

Printer-friendly Version

Interactive Discussion

Abstract

The accuracy, reliability and best practices of Ti-in-quartz thermobarometry ("TitaniQ") in greenschist facies rocks have not been established. To address these issues we measured Ti concentrations in rutile-bearing samples of moderately deformed, par-
5   tially recrystallized quartzite and vein quartz from Taiwan's Hsüehshan range. The spread of Ti concentrations of recrystallized grains in quartzite correlates with recrystallized grain size. Recrystallized quartz (grain size ~300µm) that formed during early deformation within the biotite stability field shows a marked increase in intermediate Ti-concentration grains (~1–10 ppm) relative to detrital porphyroclasts (Ti ~0.1–200 ppm).
10 Fine recrystallized quartz (~5% of the samples by area, grain size ~10–20µm) has a further restricted Ti concentration peaking at 0.8–2 ppm. This trend suggests equilibration of Ti in recrystallized quartz with a matrix phase during deformation and cooling. Vein emplacement and quartzite recrystallization are independently shown to have occurred at 250–350 °C and 300–410 °C respectively, lithostatic pressure ~5 kbar, and
15 hydrostatic fluid pressure. Estimates of the accuracy of TitaniQ at these conditions depend on whether lithostatic or fluid pressure is used in the TitaniQ calibration. Using lithostatic pressure, Ti concentrations predicted by the Thomas et al. (2010) TitaniQ calibration are within error of Ti concentrations measured by SIMS. If fluid pressure is used, predicted temperatures are ~30–40 °C too low. TitaniQ has potential to yield
20 accurate PT information for vein emplacement and dynamic recrystallization of quartz at temperatures as low as ~250 °C, however clarification of the relevant pressure term and further tests in rutile-present rocks are warranted.

1   Introduction

Titanium-in-quartz thermobarometry (referred to hereafter as TitaniQ; Wark and Wat-
25 son, 2006; Thomas et al., 2010; Huang and Audétat, 2012) has significant potential as a tool for constraining pressure and temperature of deformation independently of

Title Page

Abstract | Introduction

Conclusions | References

Tables | Figures

|◄ | ►|

◄ | ►

Back | Close

Full Screen / Esc

Printer-friendly Version

Interactive Discussion

major-element exchange thermobarometers. TitaniQ is based on the temperature- and pressure-dependent substitution of Ti for Si in quartz in the presence of rutile or other Ti-bearing phases. Previous workers have found reasonable consistency be- tween TitaniQ and traditional thermobarometry in metamorphic rocks at temperatures above ∼500 °C (Rusk et al., 2008; Spear and Wark, 2009; Storm and Spear, 2009; Pennacchioni et al., 2010; Grujic et al., 2011; Menegon et al., 2011); though see also Kawasaki and Osanai (2008) and Raimondo et al. (2011). At lower temperatures results are less clear: Kohn and Northrup (2009), Peterman and Grove (2010), Rasmussen et al. (2011), and Behr and Platt (2011) used TitaniQ to estimate temperatures as low as 280 °C in some samples, however the accuracy of these results has not been system- atically verified with independent PT constraints. Additionally, Grujic et al. (2011) found that Ti concentrations in quartz in low-temperature mylonites were not reset during dy- namic recrystallization, and Behr and Platt (2011) found both significantly higher and lower Ti-concentrations than expected in more than a third of their samples. These re- sults are all challenged by Huang and Audétat (2012), who found a crystallization-rate dependence of the thermobarometer and claim that temperatures should be 100 °C (or more) higher than those calculated in the above-cited examples. We note below however that crystallization rate did not affect Ti concentration in the experiments of Thomas et al. (2010), calling into question the results of Huang and Audétat (2012).

The above studies raise significant questions regarding the use of TitaniQ for esti- mating temperature and pressure in greenschist facies rocks: Does quartz dynamically recrystallized at low temperatures equilibrate with respect to Ti concentration? If so, how do results depend on timescale, strain, and lithology? Does equilibration depend on recrystallization mechanism (Grujic et al., 2011)? How well does TitaniQ perform when extrapolated >400 °C beyond its experimental calibration? Are anamolous results observed in rutile-absent rocks a result of wide-ranging Ti activity, TitaniQ miscalibra- tion, or other factors?

We studied partially recrystallized quartz in rutile-bearing rocks from the Hsüehshan range of central Taiwan. The Hsüehshan range has a relatively simple and

well-constrained deformation history at greenschist facies conditions (e.g. Beyssac et al., 2007). We supplement and describe available PT constraints, quantify changes in Ti concentration associated with recrystallization, compare results to the predictions of TitaniQ, and make recommendations for future development and use of Ti-in-quartz
5 thermobarometry.

2 Geologic background

Taiwan's Hsüehshan range (Figs. 1 and 2) is comprised of lithified coarse- to medium-grained sands and muds deposited in the Chinese continental margin during early Tertiary rifting (Ho, 1988). Hsüehshan range strata experienced minor extensional de-
10 formation and associated quartz veining during rifting (Tillman et al., 1992; Clark et al., 1993). An unconformity near the latitude of the study area at ~6.5 Ma separates these passive margin rocks from a foreland overlap sequence and marks the onset of colli-sion of the Luzon volcanic arc with the Chinese continental margin (Lin et al., 2003). In the Hsüehshan range, deformation associated with collision is marked by upright
15 folds (e.g. Fig. 3), subvertical cleavage, and pressure shadows indicative of co-axial deformation and horizontal compression (Clark et al., 1993; Tillman and Byrne, 1995).
    Metamorphism throughout the Hsüehshan range is greenschist facies, with high-est reported temperatures of ~475 °C reached near the core of the Tachien anticline (Fig. 2; Beyssac et al., 2007) based on Raman spectroscopy of carbonaceous mate-
20 rial ("RSCM", Fig. 2c). Temperatures were at or near peak conditions at the onset of deformation. Beyssac et al. (2007) suggested that peak temperatures were acquired under "static" conditions prior to collision since peak temperatures based on traditional metamorphic phase equilibria are lower than those indicated by RSCM (Beyssac et al., 2007) and deformation facilitates metamorphic recrystallization but has relatively little
25 effect on RSCM. Beyssac et al. (2007) and Chen et al. (2011) additionally point to a correlation between RSCM temperature and stratigraphic depth in uplifted strata as evi-dence that collisional-deformation postdated peak metamorphic conditions. We provide

Title Page

Abstract | Introduction

Conclusions | References

Tables | Figures

◄ | ►|

◄ | ►

Back | Close

Full Screen / Esc

Printer-friendly Version

Interactive Discussion

evidence below that temperatures were at least ~400 °C in the core of the Tachien anticline at the onset of deformation. Potential PT paths and available thermochronologic data are depicted in Fig. 4.

3 Methods

Thin sections were made from 50 samples of quartzite and quartz veins. Eight representative samples were selected for further study. The eight were polished, cleaned with isopropyl alcohol and coated with ~30 nm Au. Ti concentrations in quartz were analyzed on the Cameca 7f Secondary Ion Mass Spectrometer (SIMS) at the California Institute of Technology using a $^{16}O^-$ primary ion beam. In the first of four sessions we used a beam current of 4–5 nA, a mass resolving power of ~3000, and analyzed masses ^{27}Al, ^{28}Si, ^{40}Ca, ^{47}Ti, ^{48}Ti, ^{49}Ti and ^{56}Fe. In the remaining sessions we used a beam current of 7–30 nA, a mass resolving power of ~4000, and analyzed masses ^{27}Al, ^{30}Si, ^{44}Ca, ^{47}Ti and ^{49}Ti. Prior to each analysis we rastered for 60 s over a 50 × 50 μm area. We used a field aperture of 100 μm to avoid surface contamination. In an early set of (discarded) analyses using a 400 μm aperture, Ti counts in samples containing less than ~1 ppm Ti steadily decreased over >1200 s and failed to reach Ti concentrations later found using a 100 μm aperture. No temporal decay in Ti-contamination was evident using the 100 μm aperture. Effective spot size using the small aperture is 8–10 μm.

Raw data were minimally filtered. We inspected and compared trends in element ratios for each analysis and removed 11 spots (of 560 total) that could be shown with reasonable certainty to have intersected non-quartz phases. This judgment call was made when two or three trace elements at the same spot were highly irregular or when high Ti concentration coincided with petrographic evidence that the beam encountered non-quartz phases. Because of the difficulty in confidently distinguishing micro- or nano-inclusions encountered in a SIMS analysis from quartz (which could contain fine-scale compositional anomalies), we did not filter out occasional mass cycles with

anomalous trace element contents. Instead, all mass cycles were used to estimate Ti-concentrations. Our approach was to minimize subjective biases introduced by picking outliers, and use median estimates and standard errors to estimate mean values and uncertainties since these statistics are better suited for noisy data than the arithmetic mean and standard deviation.

Analyses that are likely to have intersected grain boundaries or cracks are noted in the supplementary material. We carried out a few test analyses of cracks in large, low-Ti quartz grains to determine whether they yield anomalous Ti concentrations (e.g. due to contamination during polishing). These analyses showed no higher Ti concentrations than adjacent quartz. Based on this result, and the difficulty in fine-grained recrystallized zones of establishing whether or not an analysis intersected a grain boundary, we did not discard analyses that may have intersected grain boundaries.

We used a regression line constrained through the origin (Fig. 5) to calculate Ti concentrations using National Institute of Standards (NIST) glasses 610 and 612 (434 ± 15 and 44 ± 5 ppm TiO_2 respectively, Jochum et al., 2005). To account for matrix effects between quartz and NIST glass, we used the correction factor determined by Behr et al. (2010). While such corrections could potentially change over time and under different SIMS environments, we note that the Behr et al. (2011) analyses were carried out on the same SIMS used in this study and that measured Ti/Si ratios for NIST glasses for the two studies are within error. The robustness of the correction factor is additionally suggested by its reproducibility using the same glasses and quartz standards on the SIMS at Arizona State University (W. Behr, personal communication, 2011). To check the Behr et al. (2010) correction factor, in our third analytical session we analyzed an experimentally synthesized, Ti-doped quartz (sample "Qtip 17" from Thomas et al., 2010) which has light and dark sector zones in CL images and independently known Ti concentrations of 53 ± 3 and 40 ± 2 ppm, respectively. We measure similar Ti concentrations of 56.0 ± 1 and 47.6 ± 1 ppm, respectively, using the NIST glass as standards. A regression line based on these results instead of the NIST glasses would shift our results only $\sim 10\,^{\circ}$C lower. As a Ti-blank, we used Herkimer "Diamond", a

Full Screen / Esc

Printer-friendly Version

Interactive Discussion

natural quartz containing <6 ppb Ti (Kohn and Northrup, 2009). Our analyses of this natural blank gave apparent concentrations of 15 ± 20 and 31 ± 42 ppb in session 1. The higher beam current used in later sessions however allowed us to resolve an apparent concentration of ~ 4–5 ± 2 ppb in the blank, consistent with previous work (Kohn and Northrup, 2009). No blank correction was made since these values are minimal and consistent with the expected Ti concentration of Herkimer diamond estimated by Kohn and Northrup (2009).

The TitaniQ calibration of Wark and Watson (2006) was based on experiments carried out at a uniform pressure of 10 kbar. Later experiments by Thomas et al. (2010) found a significant pressure dependence captured by the expression

$$RT \ln X_{TiO_2}^{quartz} = -60\,952 + 1520 \cdot T\,(K) - 1741 \cdot P\,(kbar) + RT \ln a_{TiO_2} \qquad (1)$$

where R is the gas constant 8.3145 J K^{-1}, T is temperature in Kelvin, $X_{TiO_2}^{quartz}$ is the mole fraction of TiO$_2$ in quartz, and a_{TiO_2} is the activity of TiO$_2$ in the system. Huang and Audétat (2012) found that Ti concentrations in experimentally grown quartz additionally correlate with crystallization rate, and present the relationship

$$\log Ti\,(ppm) = -0.27943/T - 660.53 \cdot (P^{0.35}/T) + 5.6459 \qquad (2)$$

based on their slowest experiments, with T given in Kelvin and P in kbar. Unless otherwise noted, TitaniQ temperatures reported in the paper are based on the Thomas et al. (2010) calibration.

Because metamorphic mineral assemblages observed in the Hsüehshan range are not amenable to independent quantitative geobarometry (Beyssac et al., 2007), we assume that pressure and temperature for each analysis are linked by a geothermal gradient of $25 \pm 5^\circ$ km^{-1} (91° kbar^{-1} assuming a crustal density of 2.8 g cm^{-3}). This geothermal gradient is broadly consistent with the change of 25–30° km^{-1} in RSCM temperature with stratigraphic depth in the study area (Beyssac et al., 2007), the thermal history modeled by Simoes et al. (2007) for deep exposures of the Hsüehshan

Title Page

Abstract | Introduction

Conclusions | References

Tables | Figures

◄ | ►

◄ | ►

Back | Close

Full Screen / Esc

Printer-friendly Version

Interactive Discussion

range prior to 4 Ma (Fig. 6), and the average thermal gradient in exploration wells in Taiwan (Zhou et al., 2003). The uncertainty in the estimate of the geothermal gradient of +5 or $-5\,^\circ\mathrm{km}^{-1}$ would alter a temperature estimate of $\sim 300\,^\circ\mathrm{C}$ by -10 or $+17\,^\circ\mathrm{C}$ respectively (Fig. 6). We used a Ti activity of 1.0 since the quartzites, wall rocks of veins,
5 and some veins themselves (see Table 1) contain rutile.

Data for samples and standards are reported in a supplement. We averaged titanium concentrations based on $^{47}\mathrm{Ti}/^{30}\mathrm{Si}$ and $^{49}\mathrm{Ti}/^{30}\mathrm{Si}$ measurements to calculate reported temperatures (the average $^{47}\mathrm{Ti}/^{49}\mathrm{Ti}$ of all the data is 1.37 ± 0.01, within error of natural occurrence (1.375 ± 0.006; De Laeter et al., 2003). The uncertainties
10 in temperature and pressure given for each analysis in the supplementary material are dominated by analytical precision, but also include negligible uncertainties related to analyses of standards and the above mentioned correction factor of Behr et al. (2010). Median temperatures for recrystallized quartzite, unrecrystallized veins, and recrystallized veins are given in Table 1. The 1 sigma and standard errors given in Table 1
15 reflect only the standard deviation of the pooled analyses for a given vein or recrystallized fraction. Systematic errors resulting from uncertainty in the TitaniQ calibration and geotherm estimate are also given in Table 1. By "fully recrystallized" we refer to areas with a fairly uniform recrystallized grain size, i.e. places where the beam intersected only unambiguously new grains with clear grain boundaries (no subgrains). Sorting of
20 unrecrystallized and recrystallized quartz analyses was done under the petrographic microscope following SIMS analyses but without knowledge of the Ti content of the spots.

Cathodoluminescence (CL) images were acquired on a Zeiss 1550 VP field emission scanning electron microscope at Caltech. Photons were collected using a variable-
25 pressure secondary electron detector operated at high vacuum, 30 kV accelerating voltage and 7 nA beam current.

4 Results

4.1 Description of samples

Sampled quartz veins are generally >99 % quartz with rare fragments of wall rock, chlorite, carbonate, illmenite, rutile, fluid inclusions and pressure solution seams. The
⁵ wall rock of all the veins contains rutile; the presence or absence of rutile in veins is indicated in Table 1. The veins were collected from slate, metasiltstone, and fine- to coarse-grained quartzites, and have thicknesses ranging from 100 µm to 25 mm (Table 1). Based on the orientation criteria of Tillman et al. (1992), we sampled veins that were emplaced both before and during collision (Table 1). In three of the vein samples,
¹⁰ crosscutting relationships described below allow us to discriminate sequential information about the timing of veining and dynamic recrystallization.

Two quartzite samples (148d and 148j) were chosen for intensive analysis. They have a wide range of initial grain size: fine-grained layers have detrital grains as small as 100 µm, while coarser layers contain grains commonly as large as 3 mm.
¹⁵ The quartzite contains ∼60–80 % quartz (detrital grains of quartz, quartzite, chert and quartz schist), along with lithic fragments (predominantly volcanics and slate), detrital feldspar and mica, and metamorphic chlorite and biotite (Figs. 7 and 8). The quartzites are moderately deformed with a minimum axial strain of 0.32 (Kidder et al., 2012). Foliation in the quartzites is defined by the near-vertical, NNE-SSW striking orientation of
²⁰ flattened porphyroclasts and subgrains (Figs. 2 and 7). This fabric is indistinguishable in orientation from the collisional fabrics in neighboring slates (Fig. 2, Clark et al., 1993; Tillman and Byrne, 1995; Fisher et al., 2002).

Throughout the Hsüehshan range, quartzites and quartz veins are dynamically recrystallized with a fine grain size of 4–22 µm (e.g. Figs. 9 and 10; Kidder et al., 2012).
²⁵ Recrystallization is focused along grain boundaries and occupies only 5–10 % of the samples, allowing at least rough outlines of original detrital grains to be established in thin section. Porphyroclasts (remnants of both detrital quartz grains and coarse vein quartz grains) are irregularly flattened, have serrated grain boundaries, strong

undulose extinction, contain irregular subgrains of variable size, and contain rare deformation lamellae (Figs. 9, 10, 11). These features indicate a classification in the low temperature "bulge" recrystallization regime (Stipp et al., 2002b, 2010), a rough analogue to the experimental dislocation creep "regime 1" of Hirth and Tullis (1992).

In the core of the Hsüehshan range, the bulging recrystallization is the latest phase of dynamic recrystallization and overprints coarser recrystallized grains (∼100–400 μm), which we refer to as "midsized" grains. The midsized grains (and subgrains of similar size) have a strong oblate shape preferred orientation with long axes parallel to foliation (Figs. 7, 10, 11). While collisional deformation is clearly responsible for the shape preferred orientation of the midsized grains, their formation during collision is only confirmed by comparison with undeformed Tachien and Paileng quartzites to the east and west of the Tachien anticline where this grain size fraction is rare. The size of the midsized grains falls at the boundary between recrystallized grains interpreted to have formed by subgrain rotation recrystallization and grain boundary migration recrystallization (Stipp et al., 2010). It is likely that both processes were active since subgrains are abundant with similar size and orientation as fully recrystallized midsized grains, and petrographic evidence for migration of grain boundaries at a scale of 50–60 μm across interpreted detrital boundaries is also common (Fig. 11).

4.2 Independent constraints on temperature

The grey field shown in Fig. 2c depicts the range indicated by independent constraints on temperature for dynamic recrystallization. In the case of samples 148d and 148j this constraint brackets the formation of the fine recrystallized grains overprinting the midsized grains discussed above.

4.2.1 Minimum and maximum temperature constraints

RSCM analyses (Beyssac et al., 2007) reflect peak temperature conditions and therefore serve as maximum temperature constraints for deformation. The spatial

distribution of RSCM data from Beyssac et al. (2007) is plotted as grey diamonds in Fig. 2c. Systematic errors associated with the RSCM calibration are $\sim \pm 50\,°C$ (Beyssac et al., 2004). The formation of dynamically recrystallized quartz grains requires a minimum temperature of 250–300 °C (Voll, 1976; Dresen et al., 1997; Dunlap
5   et al., 1997; Stöckhert et al., 1999; van Daalen et al., 1999; Stipp et al., 2002b).

4.2.2 Structural constraints on quartz vein emplacement temperature

Structural observations indicate that eight of the veins we analyzed were emplaced at temperatures above those required for dynamic recrystallization (i.e. >250–300 °C). The other six veins, including pre-collisional veins, have emplacement temperatures
10   constrained only by the peak conditions indicated by RSCM (samples with blue and orange bars in Fig. 12 extending off the chart on the left). The structural constraints for the eight veins emplaced at >250–300 °C are based on the observation that the Hsüehshan range was at or near peak temperatures conditions at the onset of collision and followed a relatively monotonic cooling path thereafter (Fig. 4). By showing that
15   these veins formed during collision, but prior to cooling below temperatures at which dynamic recrystallization does not occur, we constrain their emplacement temperatures between 250 °C and peak conditions.

In sample 123b, a slate, cross-cutting relationships indicate that a vein ("vein 2") cut a strongly deformed "vein 1" following a period of deformation in which vein 1 was heavily
20   recrystallized and transposed into a vertical, collision-related cleavage (Fig. 9a). Vein 1 formed during either stages 1, 2, or 3 on Fig. 4b. Vein 2 must have been emplaced after collision but before cooling below 250 °C (i.e. during stage 3 in Fig. 4) because it shows minor dynamic recrystallization itself but also cuts a collisional fabric.

The veins in samples 004 and 131 were sampled from the hinge zones of anticlines
25   (e.g. Fig. 3) formed during collision (Tillman and Byrne, 1995). The veins formed during folding since they are concentrated in the hinge zone and have a conjugate symmetry about the fold axis (Fig. 3). Dynamic recrystallization of the veins indicates that they were emplaced prior to cooling below 250 °C.

4.2.3 Microfabric constraints on maximum deformation temperature

An additional constraint on deformation temperature can be derived using the quartz deformation mechanism map of Stipp et al. (2002a). The map links the transitions between the three laboratory-based dislocation creep regimes in quartz (Hirth and Tullis, 1992) with similar microstructures found in well-constrained natural settings, and delineates boundaries in temperature-strain rate space between the regimes. Maximum bulk strain rate in the quartzite samples was $\sim 6.3 \times 10^{-14}\,\mathrm{s}^{-1}$ (Kidder et al., 2012), yielding a maximum likely temperature for bulging recrystallization of $\sim 360\,^{\circ}$C. Uncertainties associated with this approach are significant but unquantified; we assume a value of $\pm 50\,^{\circ}$C in Fig. 2c (i.e. the upper limit of the grey field is drawn at $410\,^{\circ}$C).

4.2.4 Flow law constraint on deformation temperature

The late, overprinting dynamic recrystallization in the core of the Tachien anticline (quartzite samples 148d and 148j, grain size $\sim$13–15 μm) is coarser grained than in the region to the west where the vein samples were collected (grain size $\sim$7–12 μm; Kidder et al., 2012). The recrystallized grain size piezometer of Stipp and Tullis (2003) indicates differential stresses of $\sim$75 MPa for the Tachien anticline quartzites and $\sim$110 MPa for the samples west of the Tili fault (Kidder et al., 2012). This stress difference indicates a higher deformation temperature in the anticline core if we assume a standard dislocation creep flow law for quartzite a. We estimate a minimum temperature difference of $\sim$50 °C by using the flow law for quartzite of Hirth et al. (2001), the above stress values, and assume the same strain rate in the two areas. The uniform strain rate assumption makes the estimate a minimum, since strain rates were probably slower in the west where the rocks show less total strain. Minimum deformation temperatures for samples 148d and 148j were thus $\sim$300 °C (the minimum temperature of 250 °C required for dynamic recrystallization, plus 50 °C).

4.3 Ti concentrations

4.3.1 Veins

Ti contents for each sampled vein are shown in Fig. 12. Unrecrystallized portions of veins (unfilled bars in Fig. 12) have titanium concentrations of ∼0.2–1.0 ppm. Fully recrystallized vein quartz (filled bars in Fig. 12) have equivalent or slightly higher Ti concentrations, however in no sample is the difference in Ti concentration between recrystallized and primary vein quartz significant at a 2-sigma level (Table 1).

4.3.2 Quartzites

A high density of analyses ($N = 459$) in two quartzite samples from the core of the Tachien anticline was designed to: (1) establish potential differences in Ti concentration between undeformed remnant detrital grains and recrystallized grains (Figs. 10, 13, 14), (2) monitor potential changes in Ti concentration in quartz interpreted to have recrystallized via grain boundary migration (e.g. Figs. 11, 15), and (3) analyze quartz at various distances from the rims of porphyroclasts to document whether systematic changes in Ti content occur toward grain rims (Fig. 16). As shown in the histogram of detrital Ti concentrations in Fig. 13, unrecrystallized quartz shows a wide range of Ti concentrations from ∼0.1 to ∼200 ppm which we interpret, given slow diffusion rates of Ti in quartz (Cherniak et al., 2007), to reflect the diverse origins of the detrital quartz grains. Midsized grains have a range similar to the detrital grains, but with a higher proportion of analyses in the range ∼1–10 ppm. Fully recrystallized grains from the latest deformation phase are represented by bars filled in black in Fig. 13 and peak in the range of 0.8–2 ppm.

5 Discussion

5.1 Effect of dynamic recrystallization on Ti concentration in quartz

Titanium concentrations in quartz changed during recrystallization in the studied quartzites. Fine recrystallized grains mantling high Ti detrital quartz grains have lower Ti concentrations (Fig. 10). Early "midsized" recrystallized grains have modified Ti concentration distributions relative to detrital grains (Fig. 10): only 20 % of detrital grain analyses have intermediate Ti concentrations (1–15 ppm) while 45 % of the Ti analyses of the midsized grains fall in this range (Fig. 13). It is clear from Fig. 14 that the trend towards intermediate Ti concentrations with reduced grain size continues to the finest grain fraction.

Do these changes represent equilibration of quartz and a Ti-bearing phase or phases? Or do they simply represent homogenization of quartz to an average composition, or incomplete loss of Ti from quartz without equilibration? The pattern of decreasing range of Ti-concentration with reduced grain size in Fig. 14 suggests that as recrystallization progressively reduced grain size, Ti-concentrations in quartz both decreased in areas that originally had high Ti-concentrations, and increased in areas that initially had low Ti-concentration. We conclude that Ti was not simply evacuated from quartz, but shifted toward an intermediate value. This value, ~1–2 ppm for the finest grain size fraction, is not simply an average concentration of initial Ti concentrations in detrital quartz grains, as we estimate a spatially averaged initial Ti concentration of the detrital grains was at least 10–20 ppm. We suggest that these changes in Ti concentration in recrystallized quartz reflect equilibration between quartz and at least one other phase.

In contrast to the quartzites, recrystallization of quartz in the studied veins was not associated with significant shifts in Ti concentration (Fig. 12). This observation is discussed further below.

5.2 Mechanisms of Ti mobility

We suggest that changes in Ti concentration in quartz in our samples occurred predominantly during grain boundary migration. During grain boundary migration, quartz is dissolved along one side of a grain boundary and precipitates with a new orientation on the other side (e.g. Urai et al., 1977). This process provides the opportunity for exchange of trace elements between minerals and grain boundary fluids. When such exchange occurs, gradients in trace element concentration along grain boundaries can increase, thereby increasing their mobility. Grain boundary migration was clearly active in the quartzite samples as evidenced by the offset of crystallographic grain boundaries from interpreted detrital grains boundaries (as marked by opaque and non-quartz phases, see e.g. Fig. 11). Instances of such migration events are commonly observed petrographically, occuring in ~10–20 grains per thin section. Typical migration distances range up to ~50 µm. Figure 11 demonstrates one such location where mean Ti concentration in an interpreted recrystallized area is 14 ± 7 ppm versus 34 ± 2 ppm Ti in unrecrystallized host grain. Figure 15 compiles the results of 6 such sites where large-scale grain boundary migration is suspected. A shift to lower average Ti concentrations in the recrystallized areas is apparent. A similar conclusion was also reached by Grujic (2011) who found reset Ti in mylonitized quartz veins recrystallized at temperatures above ~540 °C.

Although predicted characteristic diffusion distances for Ti in quartz based on experimentally-based diffusion coefficients (Cherniak et al., 2007) are exceedingly small under the deformation conditions experienced by the Hsüehshan range (~0.001 µm in 2.5 m.y. at 300 °C), it is possible that diffusion processes could play a role in changing Ti concentrations (e.g. the effect of high dislocation densities and strain on diffusion in quartz is unknown). We would expect diffusion to be expressed by systematic, gradual shifts in Ti-concentration along grain rims. A few porphyroclasts show indications of such behavior, e.g. the black-circled SIMS analyses in Fig. 10, and the slight convergence in Fig. 16 to intermediate Ti concentrations at distances of

5–20 µm. While intriguing, these limited observations are insufficient to unequivocally point to diffusion, and we suggest that diffusion of Ti was probably not a significant process in the samples we studied.

While we find grain boundary migration a likely mechanism for resetting Ti in quartz in the early mid-sized grains, the fine grain size associated with the latest phase of deformation prevents a similar analysis of these grains. We note that the fine grains classify within the grain boundary bulging regime of Stipp et al. (2002b, 2010; Figs. 9, 10 and 11; Kidder et al., 2012), and hypothesize that Ti concentrations in the fine grains were reset in essentially the same fashion as we propose above for the midsized grains, i.e. migration and precipitation of Ti along migrating grain boundaries.

5.3 Bias and uncertainty of TitaniQ thermobarometry at low temperatures

A major uncertainty associated with Ti-in-quartz thermobarometry in greenschist facies rocks is the potential loss of accuracy associated with extrapolating trends from laboratory calibrations to quartz crystallized or recrystallized at temperatures many hundreds of degrees below laboratory conditions. A rough estimate of the goodness of fit of our results can be made by comparing the TitaniQ predictions of Thomas et al. (2010) and Huang and Audétat (2012) with the independent constraints depicted in Figs. 2, 12, and 13. The fit can be quantified if we assume that the TitaniQ thermometer is systematically biased by ΔT and that errors are normally distributed with a variance σ^2. We can then estimate ΔT and σ from their probability distributions computed from the estimated TitaniQ temperatures (T_o) and independent constraints on temperature T_{min} and T_{max} using:

$$\rho_i(\sigma, \Delta T) = \alpha \int_{T_{min}}^{T_{max}} \frac{1}{\sqrt{2\pi}\sigma} \exp(-\frac{(T - T_o - \Delta T)^2}{2\sigma^2}) dT \tag{3}$$

where ρ is probability, T_o is a TitaniQ temperature estimate, T is temperature, and α is a normalization factor. The product of the probabilities ρ of a group of analyses yields

a probability density function in $\sigma - \Delta T$ space. The results of pooled analyses for vein emplacement (using only the eight veins with minimum and maximum constraints on temperature) and quartzite recrystallization are given in Table 2. For vein emplacement we estimate a bias of $-22\,°C + 8/-6$ (67 % confidence interval) and $80\,°C + 8/-6$ using the Thomas et al. (2010) and Huang and Audétat (2012) calibrations respectively. For quartzite recrystallization we calculate biases of $12\,°C$ and $136\,°C$. The larger bias associated with the Huang and Audétat (2012) relationship may result from non-equilibrium effects in their experiments. The growth rate dependence they describe did not occur in the experiments of Thomas et al. (2010), whose experimental results vary significantly in grain size ($<10\,\mu m$–1 mm) and therefore growth rate, with similar Ti concentrations in crystals of various sizes in any given experiment (J. Thomas, personal communication, 2012).

The bias values calculated above using the Thomas et al. (2010) calibration are small, and considering the multiple sources of potential error, there is good accord between our results and the Thomas et al. (2010) calibration. We believe the difference in estimated bias between the veins and quartzites results in part from the higher concentration of high Ti outliers in recrystallized quartzites (note the skew of the distribution of the fully recrystallized grains in Fig. 13). This is probably due to a combination of incomplete equilibration from initial conditions (detrital grains in the Tachien sandstone are dominantly high Ti) and a higher concentration of impurities in the quartzite than the veins. While a more "hands on" approach to filtering anomalous SIMS cycles and potential outliers would reduce this difference, it would introduce a set of judgment calls needed to distinguish "real" quartz analyses and analyses of inclusions. There is no reliable procedure for distinguishing between inclusions and a high impurity concentration, and ad hoc procedures to do so reduce the ability to make meaningful comparisons between studies.

5.4 Constraints on Hsüehshan range deformation conditions and timing

The thermomechanical model of Simoes et al. (2007) required two phases of deformation to match thermochronologic and metamorphic constraints in the Hsüehshan range. The early phase is characterized by slow uplift and erosion rates throughout the orogenic wedge, and the second by underplating and increased uplift rates in the Hsüehshan range. Geologic evidence also suggests a two-phase evolution of the Hsüehshan range, with early deformation characterized by penetrative horizontal compression responsible for over 30 km of shortening (Fisher et al., 2002), and later deformation marked by out of sequence thrusts (Tillman and Byrne, 1996). We suggest that the two phases proposed by the differentresearch groups correspond to the same two geologic phases. This constrains the timing of the upright folding, subvertical cleavage, and strain markers described by Clark et al. (1993) and Tillman and Byrne (1995) to before ∼4 Ma, the timing of phase two onset in the model of Simoes et al. (2007). This age constraint is consistent with observations of dislocation creep in quartzite associated with compressional deformation (this study; Tillman and Byrne, 1995), since this deformation mechanism could not be active following cooling through the zircon fission track closure temperature of ∼200–260 °C at 2.6–2.9 Ma (Fig. 3; Liu et al., 2001). The second phase of deformation may continue to the present-day, where little or no internal shortening in the Hsüehshan range is observed (Simoes and Avouac, 2006).

Previous studies of the Hsüehshan range have documented deformation under retrograde conditions (Clark et al., 1993) and concluded that peak metamorphism of the Hsüehshan range occurred "statically", prior to collision (Beyssac et al., 2007). In the course of our study we have noted features from the core of the Tachien anticline indicating that compressional deformation began while temperatures were at or near peak conditions. First, metamorphic biotite, originally noted by Yen (1973), grew in pressure shadows oriented consistently with compressional deformation (Fig. 8). Secondly, the presence of systematically oriented midsized recrystallized grains and subgrains, and the migration of grain boundaries in the quartzite samples across distances of

50–60 µm (e.g. Fig. 11) is indicative of high-temperature grain-boundary migration re-crystallization (Stipp et al., 2002a). These features indicate temperatures of at least ~400 °C (Stipp et al., 2002a; Bucher and Grapes, 2011) at the onset of collision ~6.5 Ma (Lin et al., 2003), somewhat warmer than modeled by Simoes et al. (2007; Figs. 4 and 6). This early high-temperature deformation may have resulted from thick-ening at the toe of the orogenic wedge under ambient PT conditions prior to significant motion on the decollement beneath the Hsüehshan range.

5.5 Recommendations for future TitaniQ studies

We suggest that quartzites are generally more likely to be reset during dynamic re-crystallization than vein quartz. Grujic et al. (2011) found that Ti concentrations did not change during bulging recrystallization in mylonitic veins recrystallized at similar PT conditions as the Hsüehshan range quartzites, despite much higher strains in their rocks. We note similar behavior in the Hsüehshan range veins (Fig. 12, although here it also possible that PT conditions were constant during veining and recrystallization). The lack of resetting of Ti in recrystallized vein quartz may result from an absence or scarcity of Ti-bearing phases in veins. In the quartzite we studied, Ti-bearing phases are nearly always <200 µm from recrystallized quartz. Rutile, while present in some of our veins, is rare, and the nearest source of Ti is often wall rock several mm distant (Ta-ble 1). Future studies on veins can test this hypothesis by analyzing quartz at various distances from vein edges.

As a new technique, the applicability of TitaniQ thermobarometry is debated (e.g. Thomas and Watson, 2012; Wilson et al., 2012), and further field-based tests in well-constrained localities are warranted before Ti-concentrations in quartz can be confidently interpreted in terms of PT conditions. Many previous studies have focused on Ti-undersaturated systems, and considerable effort has been expended attempting to simultaneously determine Ti activity and test TitaniQ (e.g. Grujic et al., 2011; Wil-son et al., 2012). A priority for the next phase of field-based TitaniQ studies should be

the deconvolution of these two sources of uncertainty by carrying out studies in rocks containing rutile.

An additional uncertainty in Ti-in-quartz thermobarometry, not previously discussed, is the possibility that the relevant pressure term in the TitaniQ equation is fluid pressure rather than lithostatic pressure as has previously been assumed (though not stated, e.g. Behr and Platt, 2011; Grujic et al., 2011). In many situations these pressure terms are equal, e.g. magmas, deep crustal rocks, and the experimental capsules used to calibrate TitaniQ. Near the brittle-ductile transition however, fluid pressure may often be sub-lithostatic (e.g. Küster and Stöckhert, 1998; Townend and Zoback, 2000; Behr and Platt, 2011). In the Hsüehshan range, differential stress estimates require nearly hydrostatic fluid pressure, since effective pressure ($P_{\text{lithostatic}} - P_{\text{fluid}}$) must be greater than differential stress in order for dislocation creep and dynamic recrystallization to occur (Kohlstedt et al., 1995). Vein quartz certainly formed in the presence of fluid, and fluids may also be present along grain boundaries during grain boundary migration (e.g. Urai et al., 1977; Hippertt, 1994; Mancktelow and Pennacchioni, 2004). It is possible that Ti concentrations in quartz in these settings are a function of fluid pressure rather than lithostatic pressure. Were this the case, temperatures based on Thomas et al. (2010) would be ∼30–40 °C lower than calculated above. Used with fluid pressure, the Huang and Audétat (2012) equation would give results more consistent with the independent constraints above, however this combination significantly overpredicts temperature in higher grade rocks where fluid pressures were likely lithostatic (e.g. the data presented by Storm and Spear, 2009). Considering the importance of fluid pressure in the crust (e.g. Townend and Zoback, 2000), further exploration of the sensitivity of TitaniQ to different types of pressure is warranted.

6 Conclusions

1. Collisional deformation of quartzites in the core of the Tachien anticline began at temperatures >400 °C, and was accommodated in part by high temperature grain

boundary migration recrystallization, then by bulging recrystallization as deformation continued at lower temperatures. Quartz recrystallization and penetrative deformation occurred between ~6.5 and 4 Ma.

2. Equilibration of Ti in dynamically recrystallized quartzite occurred in <2.5 m.y., during moderate deformation (axial strain ~0.32) at temperatures ~300 °C.

3. If Ti concentrations are sensitive to lithostatic pressure, as commonly assumed, the TitaniQ calibration of Thomas et al. (2010) predicts Ti concentrations in vein quartz and recrystallized quartzite within error of independently known deformation conditions in the Hsüehshan range, whereas the more recent equation from Huang and Audétat (2012) overpredicts temperatures by ~100 °C.

4. If instead Ti concentrations are a function of fluid pressure, the Thomas et al. (2010) calibration underpredicts temperatures in the Hsüehshan range by ~30–40 °C.

Supplementary material related to this article is available online at:
http://www.solid-earth-discuss.net/4/663/2012/sed-4-663-2012-supplement.pdf.

References

Behr, W. M., Thomas, J., and Hervig, R.: Calibrating Ti concentrations in quartz on the SIMS using NIST silicate glasses with applications to the TitaniQ geothermobarometer, Am. Mineral., 96, 1100–1106, doi:10.2138/am.2011.3702, 2010.

5 Behr, W. M. and Platt, J. P.: A naturally constrained stress profile through the middle crust in an extensional terrane, Earth Planet. Sc. Lett., 303, 181–192, doi:10.1016/J.Epsl.2010.11.044, 2011.

Beyssac, O., Bollinger, L., Avouac, J. P., and Goffé, B.: Thermal metamorphism in the Lesser Himalaya of Nepal determined from Raman spectroscopy of carbonaceous material, Earth

10 Planet. Sc. Lett., 225, 233–241, 2004.

Beyssac, O., Simoes, M., Avouac, J. P., Farley, K. A., Chen, Y.-G., Chan, Y.-C., and Goffé, B.: Late Cenozoic metamorphic evolution and exhumation of Taiwan, Tectonics, 26, 1–32, 2007.

Bucher, K. and Grapes, R.: Petrogenesis of Metamorphic Rocks, 8th Edition, Springer-Verlag, 428 pp., 2011.

15 Chen, C. T., Chan, Y. C., Lu, C. Y., Simoes, M., and Beyssac, O.: Nappe structure revealed by thermal constraints in the Taiwan metamorphic belt, Terra Nova, 23, 85–91, doi:10.1111/J.1365-3121.2011.00987.X, 2011.

Cherniak, D. J., Watson, E. B., and Wark, D. A.: Ti diffusion in quartz, Chem. Geol., 236, 65–74, doi:10.1016/J.Chemgeo.2006.09.001, 2007.

20 Clark, M. B., Fisher, D. M., Lu, C.-Y., and Chen, C.-H.: Kinematic analyses of the Hsüehshan range, Taiwan: A large-scale pop-up structure, Tectonics, 12, 205–217, 1993.

De Laeter, J. R., Bohlke, J. K., De Bievre, P., Hidaka, H., Peiser, H. S., Rosman, K. J. R., and Taylor, P. D. P.: Atomic weights of the elements: Review 2000 – (IUPAC technical report), Pure Appl. Chem., 75, 683–800, 2003.

25 Dresen, G., Duyster, J., Stockhert, B., Wirth, R., and Zulauf, G.: Quartz dislocation microstructure between 7000 m and 9100 m depth from the Continental Deep Drilling Program KTB, J. Geophys. Res., 102, 18443–18452, 1997.

Dunlap, W., Hirth, G., and Teyssier, C.: Thermomechanical evolution of a ductile duplex, Tectonics, 16, 983–1000, 1997.

30 Fisher, D. M., Lu, C.-Y., and Chu, H. T.: Taiwan Slate Belt: Insights into the ductile interior of an arc-continent collision, in: Geology and Geophysics of an Arc-Continent Collision, Taiwan, edited by: Byrne, T. and Liu, C. S., Geol. S. Am. S., Boulder, Colorado, 358, 93–106, 2002.

Application of titanium-in-quartz thermobarometry

S. Kidder et al.

Title Page

Abstract	Introduction
Conclusions	References
Tables	Figures

|◀| ▶|

◀ | ▶

Back | Close

Full Screen / Esc

Printer-friendly Version

Interactive Discussion

Grujic, D., Stipp, M., and Wooden, J. L.: Thermometry of quartz mylonites: Importance of dynamic recrystallization on Ti-in-quartz reequilibration, Geochem. Geophy. Geosy., 12, Q06012, doi:10.1029/2010GC003368, 2011.

Hippertt, J.: Grain boundary microstructures in micaceous quartzite: significance for fluid movement and deformation processes in low metamorphic grade shear zones, J. Geol., 102, 331–348, 1994.

Hirth, G. and Tullis, J.: Dislocation creep regimes in quartz aggregates, J. Struct, Geol., 14, 145–159, 1992.

Hirth, G., Teyssier, C., and Dunlap, W.: An evaluation of quartzite flow laws based on comparisons between experimentally and naturally deformed rocks, Int. J. Earth Sci. (Geol. Rundsch.), 90, 77–87, 2001.

Ho, C. S.: An introduction to the geology of Taiwan: explanatory text of the geologic map of Taiwan, 2nd ed., Central Geological Survey, Ministry of Economic Affairs, Taipei, Taiwan, Republic of China, xiii, 192 pp., 1988.

Huang, R. and Audétat, A.: The titanium-in-quartz (TitaniQ) thermobarometer: A critical examination and re-calibration, Geochim. Cosmochim. Ac., 84, 75–89, doi:10.1016/j.gca.2012.01.009, 2012.

Jochum, K., Nohl, U., Herwig, K., Lammel, E., Stoll, B., and Hofmann, A.: GeoReM: A new geochemical database for reference materials and isotopic standards, Geostandard. Newslett., 22, 7–13, 2005.

Kawasaki, T. and Osanai, Y.: Empirical thermometer of TiO2 in quartz for ultrahigh-temperature granulites of East Antarctica, Geological Society, London, Special Publications, 308, 419–430, doi:10.1144/sp308.21, 2008.

Kidder, S., Avouac, J. P., and Chan, Y. C.: Constraints from rocks in the Taiwan orogen on crustal stress levels and rheology, J. Geophys. Res., accepted, 2012.

Kohlstedt, D. L., Evans, B., and Mackwell, S. J.: Strength of the lithosphere–constraints imposed by laboratory experiments, J. Geophys. Res.-Sol. Ea., 100, 17587–17602, 1995.

Kohn, M. J. and Northrup, C. J.: Taking mylonites' temperatures, Geology, 37, 47–50, doi:10.1130/G25081A.1, 2009.

Küster, M. and Stöckhert, B.: High differential stress and sublithostatic pore fluid pressure in the ductile regime – microstructural evidence for short-term post-seismic creep in the Sesia Zone, Western Alps, Tectonophysics, 1998, 263–277, 1998.

Lin, A. T., Watts, A. B., and Hesselbo, S. P.: Cenozoic stratigraphy and subsidence history of the South China Sea margin in the Taiwan region, Basin Res., 15, 453–478, doi:10.1046/j.1365-2117.2003.00215.x, 2003.

Liu, T. K., Hsieh, S., Chen, Y. G., and Chen, W. S.: Thermo-kinematic evolution of the Taiwan oblique-collision mountain belt as revealed by zircon fission track dating, Earth Planet. Sc. Lett., 186, 45–56, 2001.

Mancktelow, N. S. and Pennacchioni, G.: The influence of grain boundary fluids on the microstructure of quartz-feldspar mylonites, J. Struct. Geol., 26, 47–69, doi:10.1016/s0191-8141(03)00081-6, 2004.

Menegon, L., Nasipuri, P., Stünitz, H., Behrens, H., and Ravna, E.: Dry and strong quartz during deformation of the lower crust in the presence of melt, J. Geophys. Res., 116, B10410, doi:10.1029/2011jb008371, 2011.

Pennacchioni, G., Menegon, L., Leiss, B., Nestola, F., and Bromiley, G.: Development of crystallographic preferred orientation and microstructure during plastic deformation of natural coarse-grained quartz veins, J. Geophys. Res.-Sol. Ea., 115, B12405, doi:10.1029/2010jb007674, 2010.

Peterman, E. M. and Grove, M.: Growth conditions of symplectic muscovite plus quartz: Implications for quantifying retrograde metamorphism in exhumed magmatic arcs, Geology, 38, 1071–1074, doi:10.1130/G31449.1, 2010.

Raimondo, T., Clark, C., Hand, M., and Faure, K.: Assessing the geochemical and tectonic impacts of fluid-rock interaction in mid-crustal shear zones: a case study from the intracontinental Alice Springs Orogen, central Australia, J. Metamorph. Geol., 29, 821–850, doi:10.1111/j.1525-1314.2011.00944.x, 2011.

Rasmussen, B., Fletcher, I. R., Muhling, J. R., Gregory, C. J., and Wilde, S. A.: Metamorphic replacement of mineral inclusions in detrital zircon from Jack Hills, Australia: Implications for the Hadean Earth, Geology, 39, 1143–1146, doi:10.1130/g32554.1, 2011.

Rusk, B. G., Lowers, H. A., and Reed, M., H.: Trace elements in hydrothermal quartz: Relationships to cathodoluminescent textures and insights into vein formation, Geology, 36, 547–550, 2008.

Sella, G. F., Dixon, T. H., and Mao, A. L.: REVEL: A model for recent plate velocities from space geodesy, J. Geophys. Res.-Sol. Ea., 107, 2081, doi:10.1029/2000jb000033, 2002.

Title Page

Abstract | Introduction

Conclusions | References

Tables | Figures

◀◀ | ▶▶

◀ | ▶

Back | Close

Full Screen / Esc

Printer-friendly Version

Interactive Discussion

Simoes, M. and Avouac, J. P.: Investigating the kinematics of mountain building in Taiwan from the spatiotemporal evolution of the foreland basin and western foothills, J. Geophys. Res., 111, 1–25, 2006.

Simoes, M., Avouac, J. P., Beyssac, O., Goffé, B., Farley, K. A., and Chen, Y.-G.: Mountain building in Taiwan: A thermokinematic model, J. Geophys. Res., 112, 1–25, 2007.

Spear, F. S. and Wark, D. A.: Cathodoluminescence imaging and titanium thermometry in metamorphic quartz, J. Metamorph. Geol., 27, 187–205, 2009.

Stipp, M. and Tullis, J.: The recrystallized grain size piezometer for quartz, Geophys. Res. Lett., 30, 2088, doi:10.1029/2003GL018444, 2003.

Stipp, M., Stunitz, H., Heilbronner, R., and Schmid, S. M.: Dynamic recrystallization of quartz: correlation between natural and experimental conditions, Geol. Soc. Spec. Publ., 200, 171–190, 2002a.

Stipp, M., Stünitz, H., Heilbronner, R., and Schmid, S. M.: The eastern Tonale fault zone: a 'natural laboratory' for crystal plastic deformation of quartz over a temperature range from 250 to 700 °C, J. Struct. Geol., 24, 1861–1884, 2002b.

Stipp, M., Tullis, J., Scherwath, M., and Behrmann, J. H.: A new perspective on paleopiezometry: Dynamically recrystallized grain size distributions indicate mechanism changes, Geology, 38, 759–762, doi:10.1130/G31162.1, 2010.

Stöckhert, B., Brix, M. R., Kleinschrodt, R., Hurford, A. J., and Wirth, R.: Thermochronometry and microstructures of quartz – comparison with experimental flow laws and predictions on the temperature of the brittle-plastic transition, J. Struct. Geol., 21, 351–369, 1999.

Storm, L. C. and Spear, F. S.: Application of the titanium-in-quartz thermometer to pelitic migmatites from the Adirondack Highlands, New York, J. Metamorph. Geol., 27, 479–494, doi:10.1111/j.1525-1314.2009.00829.x, 2009.

Thomas, J. and Watson, E.: Application of the Ti-in-quartz thermobarometer to rutile-free systems. Reply to: A comment on: 'TitaniQ under pressure: the effect of pressure and temperature on the solubility of Ti in quartz', Contributions to Mineralogy and Petrology, in press, doi:10.1007/s00410-012-0761-5, 2012.

Thomas, J. B., Watson, E. B., Spear, F. S., Shemella, P. T., Nayak, S. K., and Lanzirotti, A.: TitaniQ under pressure: the effect of pressure and temperature on the solubility of Ti in quartz, Contrib. Mineral. Petr., 160, 743–750, doi:10.1007/s00410-010-0505-3, 2010.

Tillman, K. S., Byrne, T. B., and Lu, C.-Y.: Pre-collision extensional structures from the central range, Taiwan: implications for the kinematic evolution of the South China Margin, Acta Geol. Taiwan., 30, 11–26, 1992.

Tillman, K. S. and Byrne, T. B.: Kinematic Analysis of the Taiwan Slate Belt, Tectonics, 14, 322–341, 1995.

Tillman, K. S. and Byrne, T. B.: Out-of-sequence thrusting in the Taiwan Slate Belt, J. Geol. Soc. China, 39, 189–208, 1996.

Townend, J. and Zoback, M. D.: How faulting keeps the crust strong, Geology, 28, 399–402, 2000.

Tsao, S. J.: The geological significance of illite crystallinity, zircon fission-track ages and K-Ar ages of metasedimentary rocks of the Central Range, Ph.D., National Taiwan University, Taipei, 272 pp., 1996.

Urai, J. L., Means, W. D., and Lister, G. S.: Dynamic recrystallization of minerals, in: Mineral and rock deformation: laboratory studies. The Paterson Volume. Geophysical Monograph 36, edited by: Hobbs, B. E. and Heard, H. C., American Geophysical Union, Washington, DC, 161–199, 1977.

van Daalen, M., Heilbronner, R., and Kunze, K.: Orientation analysis of localized shear deformation in quartz fibres at the brittle-ductile transition, Tectonophysics, 303, 83–107, 1999.

Voll, G.: Recrystallization of quartz, biotite and feldspars from Erstfeld to the Leventina nappe, Swiss Alps, and its geological significance, Schweizer Miner. Petrog., 56, 641–647, 1976.

Wark, D. A. and Watson, B.: TitaniQ: a titanium-in-quartz geothermometer, Contrib. Mineral. Petr., 2006, 743–754, 2006.

Wilson, C. J. N., Seward, T. M., Allan, A. S. R., Charlier, B. L. A., and Bello, L.: A comment on: "TitaniQ under pressure: the effect of pressure and temperature on the solubility of Ti in quartz", by: Thomas, J. B., Watson, E. B., Spear, F. S., Shemella, P. T., Nayak, S. K., and Lanzirotti, A., Contrib. Mineral. Petr., in press, doi:10.1007/s00410-012-0757-1, 2012.

Yen, T. P.: The Eocene sandstones in the Hsüehshan range terrain, Northern Taiwan, P. Geol. Soc. China, 16, 97–110, 1973.

Zhou, D., Yu, H.-S., Xu, H.-H., Shi, X.-B., and Chou, Y.-W.: Modeling of thermo-rheological structure of lithosphere under the foreland basin and mountain belt of Taiwan, Tectonophysics, 374, 115–134, doi:10.1016/s0040-1951(03)00236-1, 2003.

Title Page

Abstract | Introduction

Conclusions | References

Tables | Figures

◄ | ►

◄ | ►

Back | Close

Full Screen / Esc

Printer-friendly Version

Interactive Discussion

Table 1. Summary of results. Abbreviations: ms (metasiltstone), q (quartzite), s (slate), c (collisional), pc (pre-collisional), 1σ (random error), SE (1σ standard error), Rxl (recrystallization), sys err (systematic error due to uncertainty in the geotherm and TitaniQ calibration). "Stage" refers to the quadrants depicted in Fig. 4.

Sample/ Sample Area	Type	Rutile in vein?	Host	Width (mm)	Stage	Ti (ppm) median	mean Vein T (°C)	median Vein T (°C)	1σ	sys err	N	SE	Rxl Ti (ppm) median	Rxl T (°C) mean	Rxl T (°C) median	1σ	sys err	N	SE
004/2	vein 1, c	n	ms	0.5	1, 2, 3	0.32	265	258	17.7	27.2	7	6.7	–	–	–	–	–	–	–
004/2	vein 2, c	y	ms	0.5	3	0.187	238	237	5.6	26	5	2.5	–	–	–	–	–	–	–
004/34	vein 1, c	y	ms	2	1, 2, 3	0.484	286	276	38.1	28.1	16	9.5	0.883	306.3	305	52	30	8	18.5
004/34	vein 2, c	y	ms	0.5	3	0.515	279	279	14.3	28.3	10	4.5	–	–	–	–	–	–	–
004/5	vein 1, c	n	ms	1	1, 2, 3	0.591	282	286	28.7	28.6	5	13	–	–	–	–	–	–	–
004/5	vein 2, c	n	ms	0.1	3	0.377	272	265	29.7	27.5	11	9	–	–	–	–	–	–	–
005	vein, pc	y	q	5	1, 2	0.544	309	282	77.6	28.4	6	32	0.437	275.6	272	13	28	6	5
111b/1	vein	n	q	1.1	1, 2	0.307	256	257	14.1	27.1	9	4.7	0.277	252.6	252	8	27	6	3.4
111b/2	vein	n	q	5	2, 3	1.122	313	317	17.1	30.4	5	7.6	–	–	–	–	–	–	–
123b	vein 1	y	s	4	1, 2, 3	0.303	260	256	14.5	27	10	4.6	0.426	272.2	271	21	28	14	5.48
123b	vein 2, c	n	s	25	3	0.805	303	300	39	29.5	9	13	–	–	–	–	–	–	–
123c	vein	n	q	>10	1, 2, 3	0.49	284	277	29.7	28.2	7	11	0.515	279.3	279	2	28	2	1.1
131g	vein, c	n	q	3.6	3	0.569	285	284	12.2	28.5	8	4.3	0.662	293.2	291	7	29	9	2.4
148d	q	–	–	–	–	–	–	–	–	–	–	–	1.601	365.6	336.2	69.5	31.5	35	11.7
148j	q	–	–	–	–	–	–	–	–	–	–	–	1.834	379.3	343.8	66.5	32	13	18.4
148j	vein, pc	y	q	1,9	1, 2, 3	0.715	330	295	93.3	29.2	28	18	1.237	321.5	322	24.1	30.7	9	8.0

Application of titanium-in-quartz thermobarometry

S. Kidder et al.

Table 2. Estimated bias (ΔT) and uncertainty of TitaniQ temperature estimates using the Thomas et al. (2010) and Huang and Audétat (2012, "H&A") calibrations. Positive values of bias (ΔT) indicate an overestimate by TitaniQ relative to independent constraints.

Type	Calibration	ΔT	st. dev. (σ)
quartzite recrystallization	Thomas	12 (+16/−14)	104 (+18/−16)
quartzite recrystallization	H&A	136 (+16/−20)	126 (+22/−16)
vein emplacement	Thomas	−22 (+6/−8)	52 (+8/−6)
vein emplacement	H&A	80 (+6/−8)	62 (+10/−6)

Title Page

Abstract | Introduction

Conclusions | References

Tables | Figures

|◀ | ▶|

◀ | ▶

Back | Close

Full Screen / Esc

Printer-friendly Version

Interactive Discussion
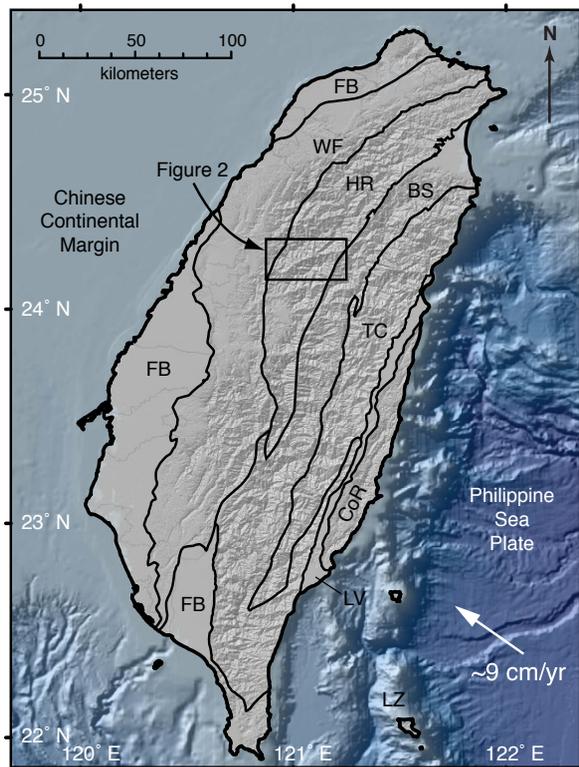
Fig. 1. Shaded relief map of Taiwan showing simplified tectonic provinces modified after Ho (1988): FB, foreland basin; WF, western foothills; HR, Hsüehshan range; BS, Backbone slates; TC, Pre-Tertiary Tananao complex; LV, Longitudinal Valley; CoR, Coastal Range; LZ, Luzon Volcanic Arc. Study area is located within the box labeled Fig. 2. Plate convergence rate (white arrow) is taken from Sella et al. (2002).

Fig. 2. (A) Geologic map of a portion of the Hsüehshan range based on Tillman and Byrne (1995) and Ho (1988) showing rock units, major structures and sample locations. **(B)** Composite cross section based on Tillman and Byrne (1995) showing their strain ellipse data from slates and our foliation analyses from quartzites. **(C)** TitaniQ temperature estimates (Thomas et al., 2010) on individual veins and independent temperature constraints are plotted relative to location on the cross section. Grey diamonds are peak temperatures from Raman spectroscopy of carbonaceous material ("RSCM"). RSCM and microstructural-based constraints discussed in the text limit quartz recrystallization to the area shaded in grey. TitaniQ estimates for vein emplacement temperatures with independent maximum and minimum temperature constraints are shown in purple. Dynamic recrystallization temperatures of quartzites and veins are shown in blue.
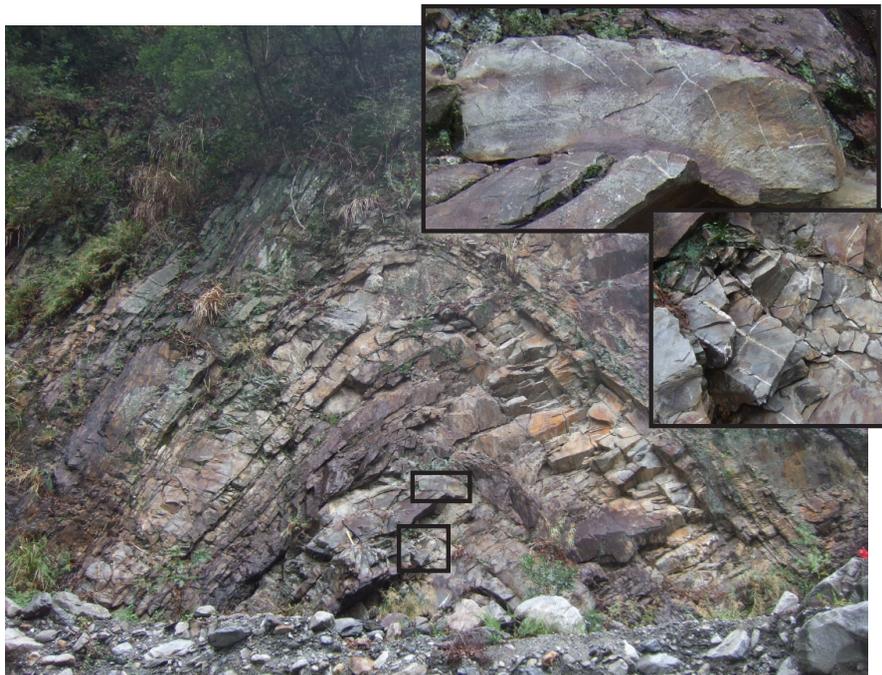
Fig. 3. Anticline within the Chiayang formation, and location of sample 131g. The outcrop is dominantly quartzite, with minor slate interbeds. Insets show examples of conjugate veins concentrated in the hinge zone of the anticline. The location of the veins indicates an origin during collision.

Title Page

Abstract | Introduction

Conclusions | References

Tables | Figures

◄ | ►►

◄ | ►

Back | Close

Full Screen / Esc

Printer-friendly Version

Interactive Discussion
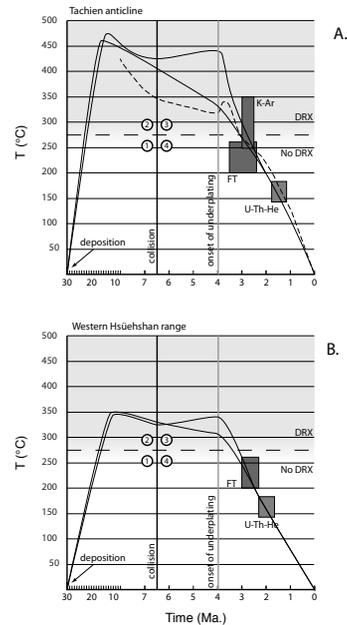
Fig. 4. Constraints on temperature-time history and possible cooling paths for **(A)** the deepest exposed levels of the Hsüehshan range where quartzites 148d and 148j were sampled, and **(B)** the cooler region to the west where the remainder of samples were collected. Cooling rates since ~3 Ma are well constrained at ~90° m.y.$^{-1}$ by zircon fission track (Liu et al., 2001), zircon U-Th-He (Beyssac et al., 2007), and white mica K-Ar data (Tsao, 1996). Note that the x-axis is compressed by a factor of 10 between 30 and 8 Ma. The dashed line reproduces the results of the thermal-kinematic model of Simoes et al. (2007). The thin black lines represent cooling paths constrained by evidence of elevated temperatures at the onset of collision. Quadrants 1, 2, 3, and 4 separate pre- and post-collision stages and stages where dynamic recrystallization (DRX) occurs (grey) or does not occur (white). Closure temperatures for K-Ar data on a set of <2 μm white mica grains span the values quoted by Tsao (1996) and a lower temperature suggested by Beyssac et al. (2007) for these data.
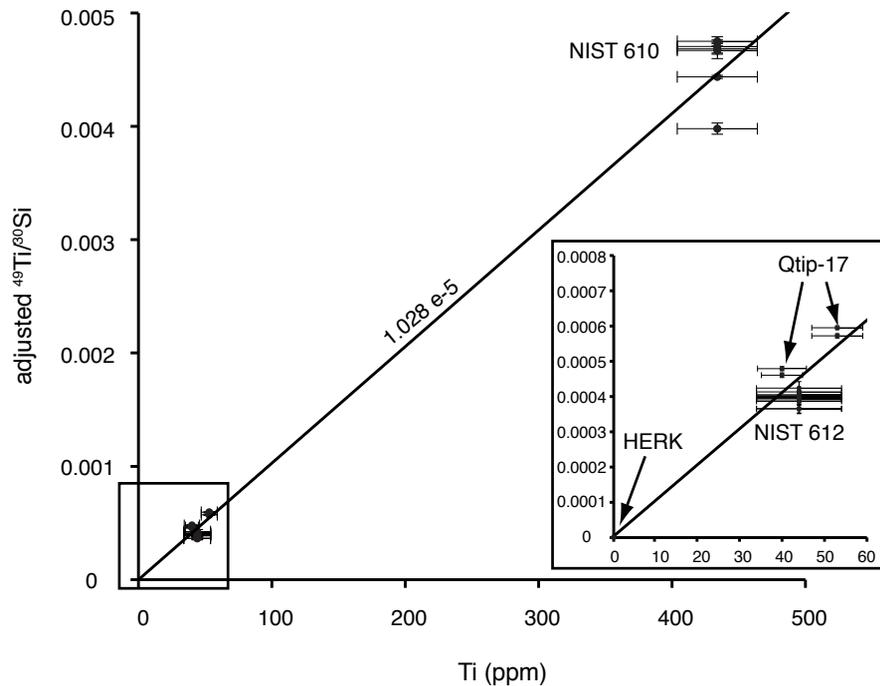
Fig. 5. Ti content of standards vs. adjusted $^{49}Ti/^{30}Si$ ratios. Measured $^{49}Ti/^{30}Si$ ratios for NIST glasses are corrected for Si concentration (multiplied by factors of 0.7 and 0.72 for NIST 610 and 612 respectively to account for differences in silica content between quartz and NIST glass) then divided by a correction factor of 0.67 (Behr et al., 2010) to enable direct comparison with NIST glasses. The plotted regression line is constrained by the origin and data for NIST glasses only. Quartz samples Qtip-17 and a sample of Herkimer "Diamond" are plotted for comparison purposes (see text). Error bars for $^{49}Ti/^{30}Si$ ratios and Ti concentrations are 2σ.
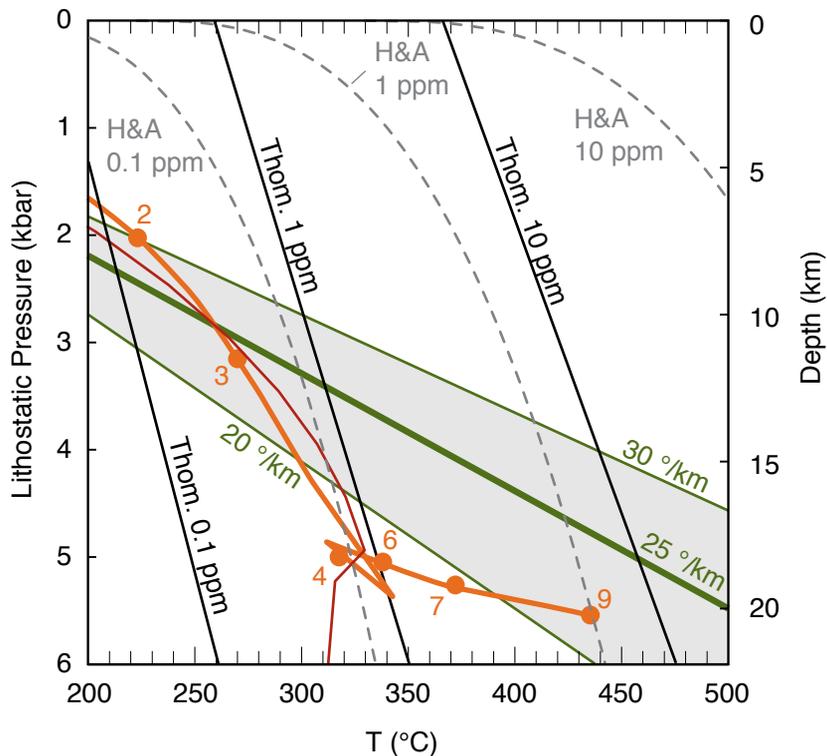
Fig. 6. Pressure-temperature plot showing the Thomas et al. (2010) and Huang and Audétat (2012) TitaniQ calibrations for 0.1, 1, and 10 ppm Ti; the 25° km^{-1} geothermal gradient assumed in our calculations with ±5° km^{-1} assumed uncertainty (gray field); the PT path for the core of the Hsüehshan range from the model of Simoes et al. (2007) (orange line) with numbers indicating ages in Ma. The geothermal gradient at 4 Ma from the thermokinematic model of Simoes et al. (2007) is shown in red.
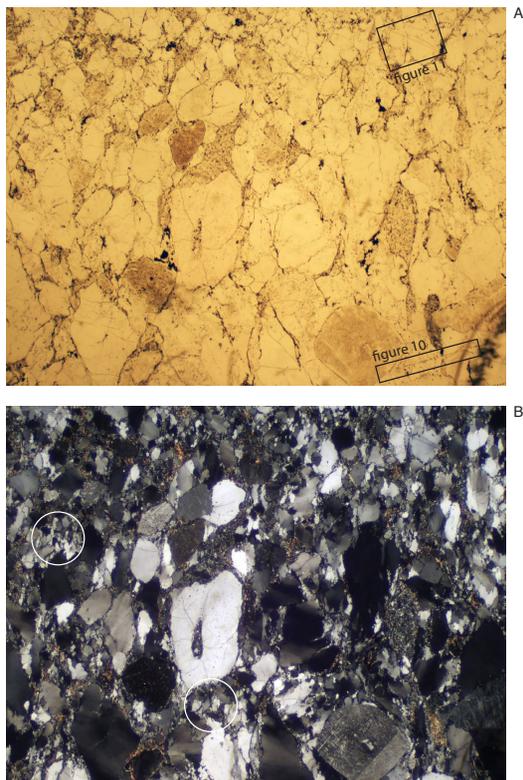
Fig. 7. Photomicrographs of sample 148d oriented with bedding horizontal and vertical tectonic foliation marked by preferred orientation of porphyroclasts and subgrains. **(A)** unpolarized. **(B)** Cross polarized. Locations of Figs. 10 and 11 are outlined in **(A)**. The white circles in **(B)** indicate two locations dominated by "midsized" recrystallized grains as discussed in the text. FOV ~ 7 mm.

Full Screen / Esc

Printer-friendly Version

Interactive Discussion
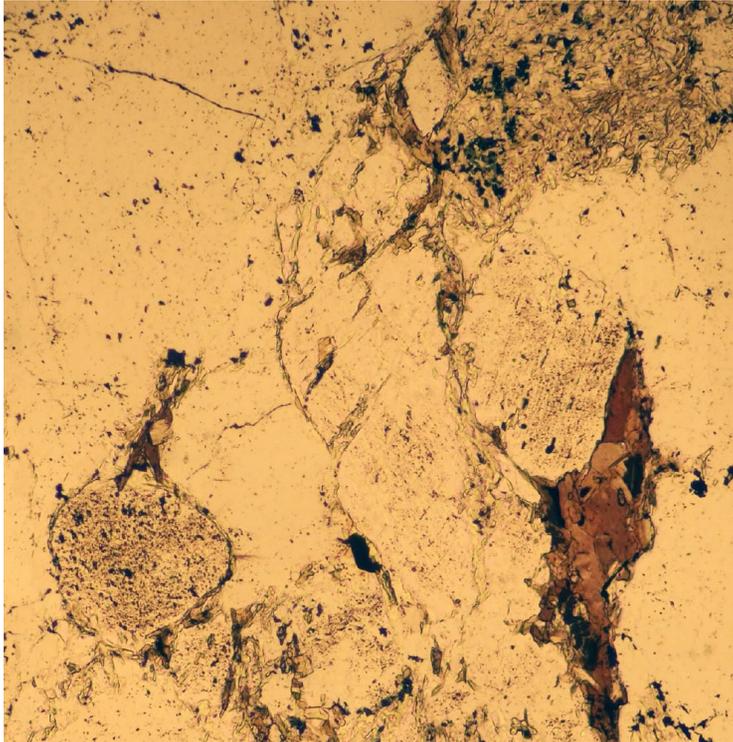
Fig. 8. Photomicrograph of sample 148d showing growth of metamorphic biotite in strain fringes on two detrital feldspar grains in the core of the Tachien anticline. Bedding and tectonic short-ening direction (WNW-ESE) are horizontal in the figure. FOV 0.9 mm.
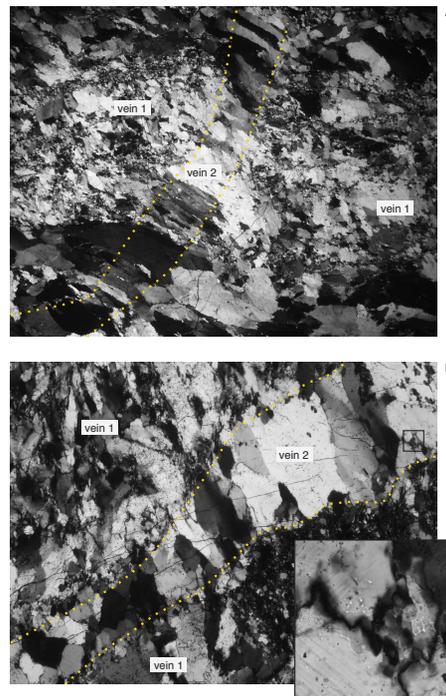
Fig. 9. Microphotographs of two samples where alternating brittle and plastic deformation can be documented. **(A)** Sample 123b showing a strongly recrystallized early vein ("vein 1") cut and offset by a later vein ("vein 2") outlined in yellow. Foliation (vertical in the field) is horizontal in the photograph. FOV ∼ 12 mm. **(B)** Photo of site 34 in sample 004, with early vein material strongly recrystallized in the upper part of the photograph. A late vein ("vein 2") running from lower left to upper right postdates dynamic recrystallization of the earlier vein. The late vein has a lower inclusion concentration and retains some crystal facets (lower left). Undulatory extinction, subgrains, and minor dynamic recrystallization (inset) of the late vein indicate it too was deformed at temperatures >250 °C. FOV ∼ 2.7 mm.

Full Screen / Esc

Printer-friendly Version

Interactive Discussion
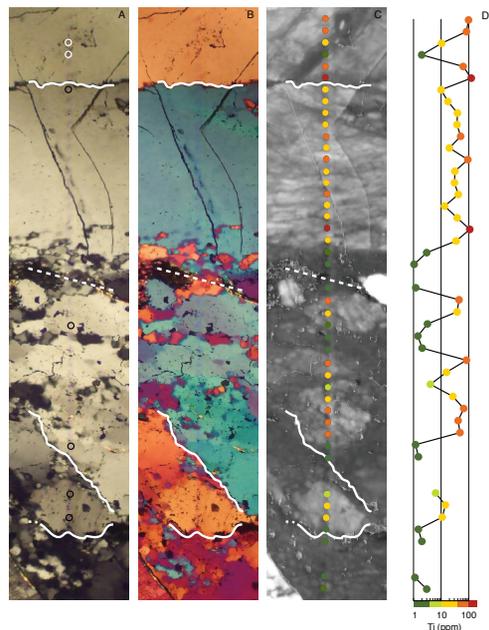
Fig. 10. Cross-polarized microphotograph **(A)**, cross-polarized microphotograph with mica-plate inserted **(B)**, and CL image **(C)** of the same area of quartzite sample 148d. **(D)** Graph of Ti concentrations for SIMS analyses. White lines on the images are detrital grain boundaries. Spacing of SIMS analyses is 25 µm. The five black-outlined spots in **(A)** are analyses where Ti concentration is notably reduced in the vicinity of grain boundaries. This trend does not hold for all grain boundaries (e.g. the edge of the top grain in the figure). Two white-outlined spots in the grain at the top of the figure show significant reduction of Ti content along a band marked by increased visible inclusions (**A** and **B**) and lower CL intensity **(C)**. This zone corresponds with a subgrain boundary visible under different polarization orientation.
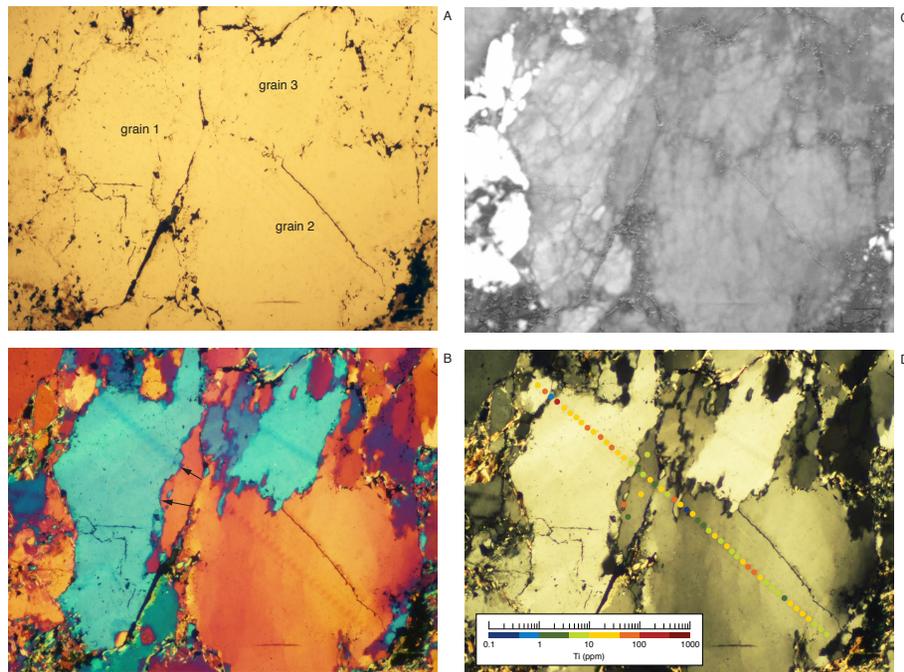
Fig. 11. Photomicrographs showing an example of a large-scale grain boundary migration. **(A)** Image taken in plain polarized light showing outlines of three labeled detrital grains. **(B)** Same image taken under cross-polarized light with the mica-plate inserted. A portion of the right side of grain 1 has been recrystallized with the same orientation as grain 2. Arrows indicate the interpreted direction and magnitude of grain boundary migration. **(C)** CL image of the same area. The recrystallized portion of grain 1 in this image has a slightly darker color than either grain 1 or 2. **(D)** Cross-polarized image showing Ti concentrations in grains 1 and 2. Ti concentrations in the recrystallized portion of grain 1 are significantly lower than the average Ti concentration of grain 1 (see text for details). Field of view: 880 µm.
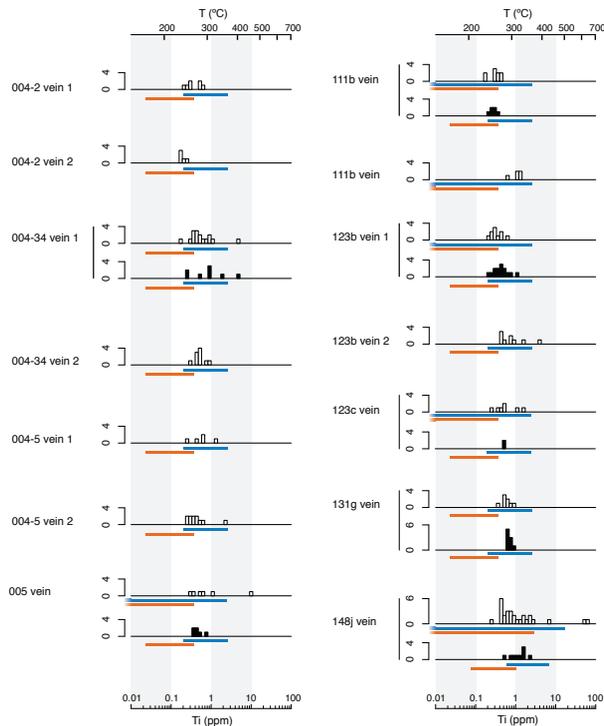
Fig. 12. Histograms for veins showing Ti content of fully recrystallized grains (black fill) and unrecrystallized or incompletely recrystallized grains (white fill). Orange and blue bars at the base of the histograms indicate the range of Ti concentrations predicted by the Huang and Audétat (2012) and Thomas et al. (2010) TitaniQ calibrations respectively based on independent temperature constraints discussed in the text. The orange and blue bars are based on a geothermal gradient between 20 and 30° km^{-1}. Temperature scale shown is based on the Thomas et al. (2010) calibration assuming a 25° km^{-1} geotherm and lithostatic fluid pressure. The figure shows good agreement between the Ti data and Thomas et al. (2010) TitaniQ calibration.
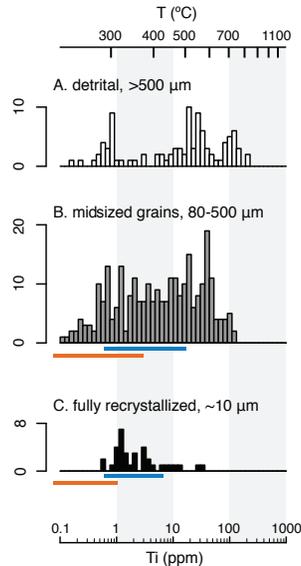
Fig. 13. Histograms for quartzites showing **(A)** Ti content of detrital grain remnants (white fill), **(B)** midsized recrystallized grains (grey fill), and **(C)** fully recrystallized fine-grained quartz (black fill). Orange and blue bars at the base of the histograms indicate the range of Ti concentrations predicted by the Huang and Audétat (2012) and Thomas et al. (2010) TitaniQ calibrations respectively based on independent temperature constraints discussed in the text. The orange and blue bars are based on a geothermal gradient between 20 and 30° km^{-1}. The histogram for detrital quartz is biased by the preferential analysis of low Ti grains, and its peaks should not therefore be strictly interpreted in terms of sedimentary provenance. Temperature scale shown is based on the Thomas et al. (2010) calibration assuming a 25° km^{-1} geotherm and lithostatic fluid pressure. Figure **(B)** shows a marked increase in intermediate Ti concentration grains relative to **(A)** indicating probable resetting of Ti in these grains. The resticted range of Ti concentrations in **(C)** relative to **(A)** suggests both gain and loss of Ti from parent quartz material (i.e. equilibration) during recrystallization. As in Fig. 12, the Thomas et al. (2010) calibration better fits the Ti data.
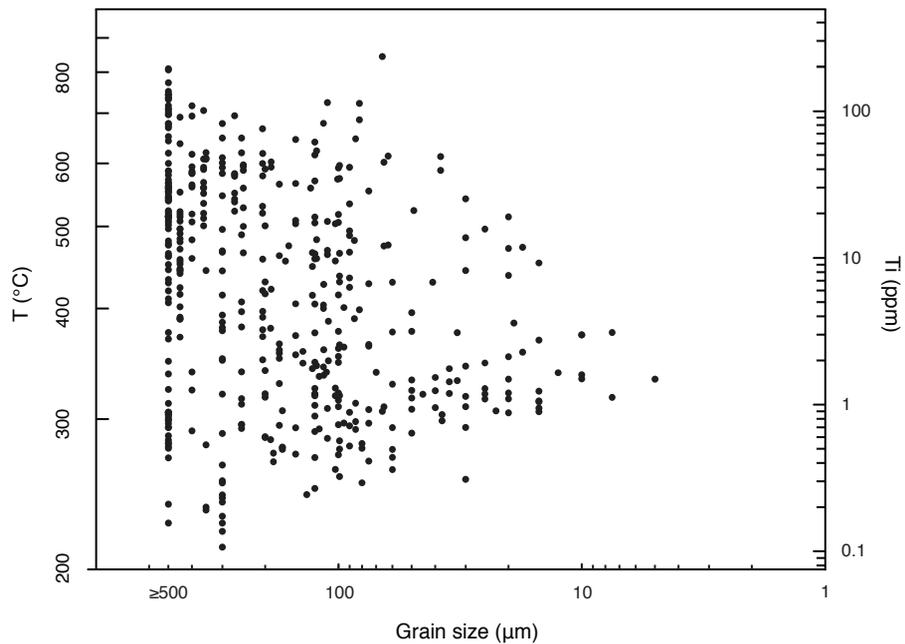
**Fig. 14.** Temperature vs. grain size for all analyses in the quartzite samples.
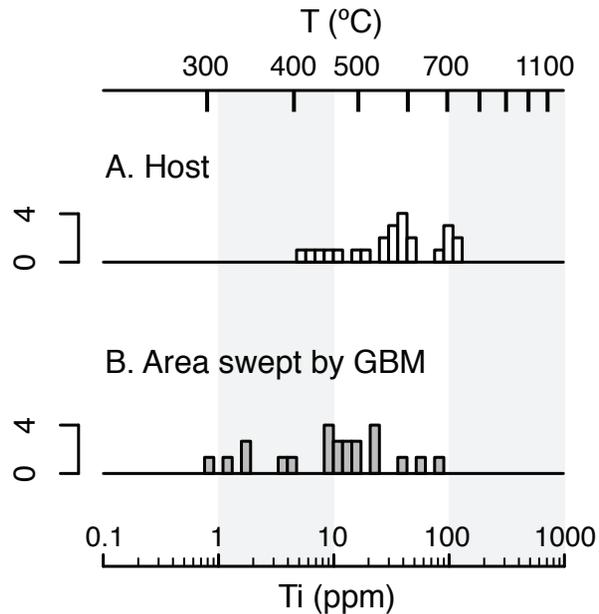
Fig. 15. Comparison of compiled Ti analyses in **(A)** six detrital porphyroclasts and **(B)** regions of the same porphyroclasts believed to have recrystallized due to grain boundary migration (GBM). An example of one such site is shown in Fig. 11. Temperature scale shown is based on Thomas et al. (2010) calibration assuming 25° km^{-1}.
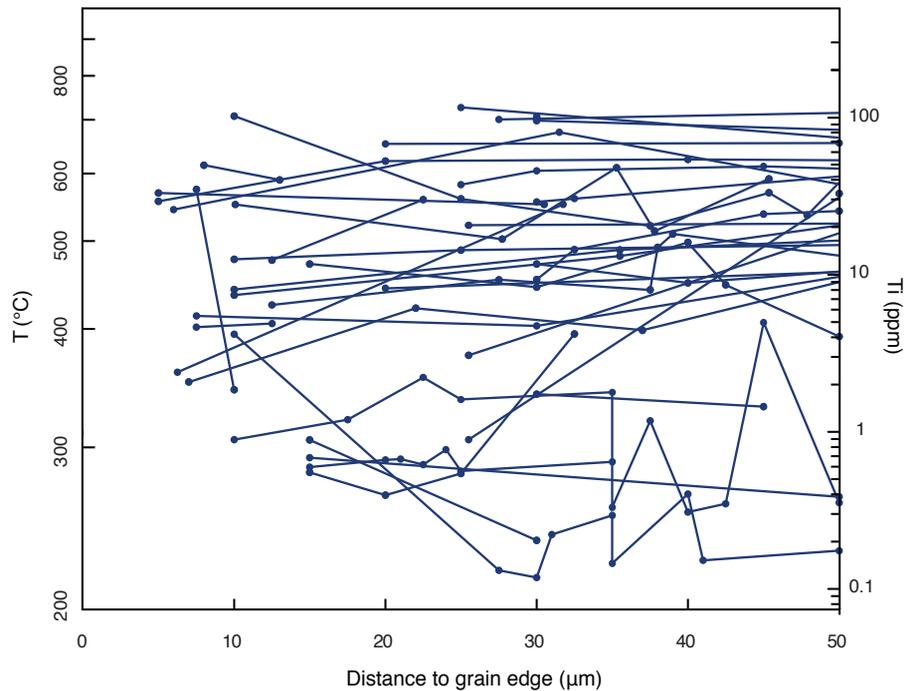
Fig. 16. Ti concentration vs. distance to grain edge in porphyroclasts.